INTERNATIONAL JOURNAL FOR NUMERICAL METHODS IN ENGINEERING
Int. J. Numer. Meth. Engng 2008; **74**:1198–1218
Published online 9 November 2007 in Wiley InterScience (www.interscience.wiley.com). DOI: 10.1002/nme.2212

On finite-strain damage of viscoelastic-fibred materials. Application to soft biological tissues

E. Peña[1,2], B. Calvo[1,2], M. A. Martínez[1,2] and M. Doblaré[1,2,*,†]

[1]*Group of Structural Mechanics and Materials Modeling, Aragón Institute of Engineering Research, University of Zaragoza, Spain*
[2]*CIBER-BBN, Networking Centre on Bioengineering, Biomaterials and Nanomedicine, Aragón Institute of Health Sciences, Spain*

SUMMARY

The aim of this paper is to introduce a fully three-dimensional finite-strain damage model for visco-hyperelastic fibrous soft tissue. The structural model is formulated using the concept of internal variables that provide a very general description of materials involving irreversible effects. Continuum damage mechanics is used to describe the softening behaviour of soft tissues under large deformation. Modelling of the viscoelastic behaviour is based on a local additive decomposition of the stress tensor into initial and non-equilibrium parts as resulted from the assumed structure of an uncoupled free energy density function. A local multiplicative decomposition of the deformation gradient into volume-preserving and dilatational parts is used which permits one to model the incompressible properties of soft biological tissues. The presented formulation and the associated algorithmic discretization were efficiently implemented into a finite element code.

In order to show the performance of the constitutive model and it's algorithmic counterpart, some simple examples are included. A more complex three-dimensional numerical application to ligament mechanics is also presented. Results show that the model is able to capture the typical stress–strain behaviour observed in fibrous soft tissues and seems to confirm the soundness of the proposed formulation. Copyright © 2007 John Wiley & Sons, Ltd.

Received 12 December 2006; Revised 4 September 2007; Accepted 5 September 2007

KEY WORDS: viscoelasticity; directional damage; internal variables; finite strains; fibred materials; finite element method

*Correspondence to: Manuel Doblaré, Mechanical Engineering Department, University of Zaragoza, Agustín de Betancourt Building, María de Luna, s/n. E-50018 Zaragoza, Spain.
†E-mail: mdoblare@unizar.es

Contract/grant sponsor: CICYT; contract/grant numbers: DPI2004-07410-C03-01, FIS2005-05020-C03-03
Contract/grant sponsor: European Commission; contract/grant number: IST-2004-27252-DeSSOS

Copyright © 2007 John Wiley & Sons, Ltd.

1. INTRODUCTION

Biological soft tissues are subjected to large deformations with negligible volume change and show a highly non-linear anisotropic mechanical response due to their internal structure [1]. The extra-cellular matrix is composed of a network of collagen fibrils and elastin fibres embedded in a viscous and quasi-isotropic ground substance [2]. Typical examples of fibred soft biological tissues are blood vessels, tendons, ligaments, cornea and cartilage [3].

The purely elastic response of ligaments is often modelled within the framework of continuum mechanics by means of the definition of a strain energy function expressed in terms of kinematic invariants, first developed by Spencer [4]. This approach was further tuned and applied to finite element simulations of soft collagenous biological tissues (see, for example, Weiss *et al.* [5], Peña *et al.* [6] for ligaments, Holzapfel *et al.* [7] for arteries and Alastrue *et al.* [8] for cornea).

Many fibred soft tissues exhibit simultaneously elastic and viscous material behaviour. The rate-dependent material behaviour of these kinds of materials has been well documented and quantified in the literature. This includes works on ligaments [9], tendons [10], blood vessels [11], cornea [12] and articular cartilage [13]. This behaviour can arise from the fluid flow inside the tissue, from the inherent viscoelasticity of the solid phase or from viscous interactions between the tissue phases [14]. Furthermore, non-physiological loads drive soft tissue to damage that may induce a strong reduction of the stiffness. Damage may arise from two possible mechanisms: tear or plastic deformation of the fibres, or biochemical degradation of the extracellular matrix from protease release associated with the observed cellular necrosis [15].

In order to obtain a realistic and complete material model, damage should be coupled with viscoelasticity to account for both inelastic features. Some computational models of viscoelastic materials with damage have been developed in the literature. Simo [16] and Govindjee and Simo [17] developed a fully three-dimensional finite-strain viscoelastic damage model using the concept of internal variables. Kaliske and Rothert [18] and Kaliske *et al.* [19] introduced a viscoelastic and elastoplastic formulation with damage also using internal variables. Canga *et al.* [20] presented a viscoelastic damage model using hereditary integrals to simulate viscoelasticity. Lin and Schomburg [21] presented a finite non-linear viscoelastic–elastoplastic material law with damage based on a set of dissipation inequalities. All these models are isotropic and were mainly applied to model rubber-like materials.

For soft tissue, only Arnoux *et al.* [22] presented a visco-hyperelastic model with damage for the knee ligaments under dynamic constraints. That model considered only pure isotropic behaviour. Several experiments have shown different behaviours for collagen fibres and ground substance in soft biological tissues [15, 23]. However and up to date, models that consider anisotropic viscous behaviour [2, 24, 25] have not been coupled with directional damage models [26, 27].

The aim of this paper is to present a fully three-dimensional finite-strain damage model for visco-hyperelastic fibrous soft tissue. Continuum damage mechanics is used to describe the softening behaviour under large deformation. This model is formulated in terms of a local additive decomposition of the stress tensor into initial and non-equilibrium parts as resulting from the assumed structure of an uncoupled free energy density function. It is stated within the framework of models with internal variables which provides a very general description of materials involving irreversible effects. Several examples under finite strains are presented in order to illustrate the good performance and the physical mechanisms inherent to such constitutive model.

Copyright © 2007 John Wiley & Sons, Ltd.

DOI: 10.1002/nme

The paper is organized as follows. In Section 2 the constitutive equations of anisotropic hyperelastic materials are briefly revised. In Section 3 the proposed anisotropic visco-hyperelastic-damage model for biological soft tissue is presented. Section 4 shows the integration algorithm for the resulting constitutive equations. The application to some examples is presented in Section 5. A comparison with experimental data and numerical simulations is also included to illustrate the effectiveness of the proposed formulation. Simple geometry examples are used to validate and easily compare different methodologies. Next, the simulation of the behaviour of the human medial collateral ligament (MCL) under non-physiological loads is discussed. Finally, Section 6 includes some concluding remarks.

2. FINITE ELASTICITY WITH UNCOUPLED VOLUME RESPONSE

As a first step towards the development of a non-linear anisotropic visco-hyperelastic-damage model, this section deals with the formulation of the finite-strain material model. To clarify the formulation it is necessary to summarize the formulation of finite-strain hyperelasticity in terms of invariants with uncoupled volumetric/deviatoric responses, first suggested in Flory [28], generalized in Simo and Taylor [29] and employed for anisotropic soft biological tissues in [5, 7, 8] among others.

Consider a continuum body with reference configuration Ω_0 at the initial reference time $t=0$. Then, a motion $\boldsymbol{\chi}$ maps this configuration to the current configuration Ω at each time t. Hence, a point $\mathbf{X}\in\Omega_0$ transforms to a point $\mathbf{x}\in\Omega$, where $\mathbf{X}$ and $\mathbf{x}$ define the respective positions of a particle in the reference and current configurations relative to a fixed set of axes. The direction of a fibre at a point $\mathbf{X}\in\Omega_0$ is defined by a unit vector field $\mathbf{m}_0(\mathbf{X})$, $|\mathbf{m}_0|=1$. It is usually assumed that, under deformation, the fibre moves with the material points of the continuum body, that is, it follows an affine deformation. Therefore, the stretch λ of the fibre defined as the ratio between its lengths at the deformed and reference configurations can be expressed as

$$\lambda\mathbf{m}(\mathbf{x},t)=\mathbf{F}(\mathbf{X},t)\mathbf{m}_0(\mathbf{X}) \tag{1}$$

where $\mathbf{m}$ is the unit vector of the fibre in the deformed configuration

$$\lambda^2=\mathbf{m}_0\cdot\mathbf{F}^{\mathrm{T}}\mathbf{F}\cdot\mathbf{m}_0=\mathbf{m}_0\cdot\mathbf{C}\mathbf{m}_0 \tag{2}$$

In (1), (2) $\mathbf{F}=\mathrm{d}\mathbf{x}/\mathrm{d}\mathbf{X}$ and $\mathbf{C}=\mathbf{F}^{\mathrm{T}}\mathbf{F}$ are the standard deformation gradient and the corresponding right Cauchy–Green strain measure. A multiplicative decomposition of $\mathbf{F}$ into *volume-changing* (*dilational*) and *volume-preserving* (*distortional*) parts is usually established as in [28, 29]

$$\mathbf{F}=J^{1/3}\bar{\mathbf{F}},\quad \mathbf{C}=J^{2/3}\bar{\mathbf{C}} \tag{3}$$

$J=\det\mathbf{F}$ being the jacobian of the motion.

The introduced kinematics for one family of fibres can be applied to other fibre families in an analogous manner. We shall denote a second preferred fibre orientation by the unit vector field $\mathbf{n}_0(\mathbf{X})$.

To characterize isothermal processes, we postulate the existence of a unique decoupled representation of the strain-energy density function Ψ [30]. Because of the directional dependence on the deformation, we require that the function Ψ explicitly depends on both the right Cauchy–Green

Copyright © 2007 John Wiley & Sons, Ltd.

DOI: 10.1002/nme

tensor $\mathbf{C}$ and the fibres directions $\mathbf{m}_0$ and $\mathbf{n}_0$ in the reference configuration. Since the sign of $\mathbf{m}_0$ and $\mathbf{n}_0$ is not significant, Ψ must be an even function of $\mathbf{m}_0$ and $\mathbf{n}_0$ and hence it may be expressed as $\Psi=\Psi(\mathbf{C},\mathbf{M},\mathbf{N})$, where $\mathbf{M}=\mathbf{m}_0\otimes\mathbf{m}_0$ and $\mathbf{N}=\mathbf{n}_0\otimes\mathbf{n}_0$ are structural tensors [4]. On the basis of the kinematic description (3), the free energy can be rewritten in decoupled form as

$$\Psi(\mathbf{C})=\Psi_{\mathrm{vol}}(J)+\bar{\Psi}(\bar{\mathbf{C}},\mathbf{M},\mathbf{N}) \tag{4}$$

where $\Psi_{\mathrm{vol}}(J)$ and $\bar{\Psi}(\bar{\mathbf{C}},\mathbf{M},\mathbf{N})$ are the given scalar-valued functions of J, $\bar{\mathbf{C}}$, $\mathbf{m}_0$ and $\mathbf{n}_0$, respectively, which describe the volumetric and isochoric responses of the material [31]. In terms of the strain invariants [4], Ψ can be written as

$$\begin{aligned}\Psi = \Psi_{\mathrm{vol}}(J)+\bar{\Psi}(&\bar{I}_1(\bar{\mathbf{C}}),\bar{I}_2(\bar{\mathbf{C}}),\bar{I}_4(\bar{\mathbf{C}},\mathbf{m}_0),\bar{I}_5(\bar{\mathbf{C}},\mathbf{m}_0),\bar{I}_6(\bar{\mathbf{C}},\mathbf{n}_0),\\ &\bar{I}_7(\bar{\mathbf{C}},\mathbf{n}_0),\bar{I}_8(\bar{\mathbf{C}},\mathbf{m}_0,\mathbf{n}_0),\bar{I}_9(\mathbf{m}_0,\mathbf{n}_0))\end{aligned} \tag{5}$$

with $\bar{I}_1$ and $\bar{I}_2$ the first two modified strain invariants of the symmetric modified Cauchy–Green tensor $\bar{\mathbf{C}}$. (Note that $I_3=J^2$ and $\bar{I}_3=1$.) Finally, the pseudo-invariants $\bar{I}_4,\ldots,\bar{I}_9$ characterize the constitutive response of the fibres [4]:

$$\begin{aligned}&\bar{I}_4=\bar{\mathbf{C}}:\mathbf{M}, \quad \bar{I}_5=\bar{\mathbf{C}}^2:\mathbf{M}\\ &\bar{I}_6=\bar{\mathbf{C}}:\mathbf{N}, \quad \bar{I}_7=\bar{\mathbf{C}}^2:\mathbf{N}\\ &\bar{I}_8=(\mathbf{m}_0\cdot\mathbf{n}_0)\mathbf{m}_0\cdot\bar{\mathbf{C}}\mathbf{n}_0, \quad \bar{I}_9=(\mathbf{m}_0\cdot\mathbf{n}_0)^2\end{aligned} \tag{6}$$

While the invariants $\bar{I}_4$ and $\bar{I}_6$ have a clear physical meaning, the square of the stretch λ in the fibres directions, the influence of $\bar{I}_5$, $\bar{I}_7$ and $\bar{I}_8$ is difficult to evaluate due to the high correlation between them. For this reason and the lack of sufficient experimental data it is usual not to include these invariants in the definition of Ψ [4]. Finally, the invariant $\bar{I}_9$ does not depend on the deformation; hence, it has not been included in (5).

We now define the constitutive equation for compressible hyperelastic materials in the standard form

$$\mathbf{S}=2\frac{\partial\Psi(\mathbf{C},\mathbf{M},\mathbf{N})}{\partial\mathbf{C}}=\mathbf{S}_{\mathrm{vol}}+\bar{\mathbf{S}}=2\frac{\partial\Psi_{\mathrm{vol}}(J)}{\partial\mathbf{C}}+2\frac{\partial\Psi_{\mathrm{iso}}(\bar{\mathbf{C}},\mathbf{M},\mathbf{N})}{\partial\mathbf{C}} \tag{7}$$

where the second Piola–Kirchhoff stress $\mathbf{S}$ consists of a purely volumetric contribution and a purely isochoric one. The associated decoupled elasticity tensor may be written as

$$\mathbb{C}=\mathbb{C}_{\mathrm{vol}}+\mathbb{C}_{\mathrm{iso}}=2\frac{\partial\mathbf{S}_{\mathrm{vol}}}{\partial\mathbf{C}}+2\frac{\partial\mathbf{S}_{\mathrm{iso}}}{\partial\mathbf{C}} \tag{8}$$

The Cauchy stress tensor $\boldsymbol{\sigma}$ and the elasticity tensor in the spatial description $\mathbb{c}$ is $1/J$ times the push forward of $\mathbf{S}$ or $\mathbb{C}$, respectively [31, 32]

$$\boldsymbol{\sigma}=J^{-1}\boldsymbol{\chi}_*(\mathbf{S}), \quad \mathbb{c}=J^{-1}\boldsymbol{\chi}_*(\mathbb{C}) \tag{9}$$

For a more detailed derivation of the material and spatial elasticity tensors for fully incompressible or compressible fibred hyperelastic materials and their explicit expressions, see i.e. [3, 4].

Copyright © 2007 John Wiley & Sons, Ltd.

DOI: 10.1002/nme

3. PHENOMENOLOGICAL VISCOELASTIC-DAMAGE MODEL

To motivate the coupled viscoelastic-damage model, we consider the finite-strain anisotropic viscoelastic constitutive behaviour proposed by Peña *et al.* [25] and the directional damage model proposed by Calvo *et al.* [26]. Damage and viscoelastic phenomena are here assumed to affect only the isochoric elastic part of the deformation, as proposed by Simo [16].

3.1. Anisotropic viscoelastic-damage approach

The ideas discussed in [25, 26] can be readily extended to account for viscous and damage effects within the same approach. The free energy density can be rewritten as the augmented functional:

$$\Psi(\mathbf{C},\mathbf{M},\mathbf{N},D_k,\mathbf{Q}_{ik}) = \Psi^0_{\text{vol}}(J) + \sum_{k=m,f_1,f_2}(1-D_k)\bar{\Psi}^k_0 - \frac{1}{2}\sum_{i=1}^{N}\sum_{k=m,f_1,f_2}(\bar{\mathbf{C}}:\mathbf{Q}_{ik}) + \Xi\left(\sum_{i=1}^{N}\sum_{k=m,f_1,f_2}\mathbf{Q}_{ik}\right) \tag{10}$$

where $\mathbf{Q}_{ik}$ may be interpreted as non-equilibrium stresses, in the sense of non-equilibrium thermodynamics, and remain unaltered under superposed spatial rigid body motions [33]. $\mathbf{Q}_{im}$ are the isotropic contribution of the matrix material associated with the invariants I_1 and I_2, and $\mathbf{Q}_{if_1}, \mathbf{Q}_{if_2}$ are the anisotropic contributions of the two families of fibres associated with the invariants $I_4, \ldots, I_9$ [25]. Finally $(1-D_k)$ are known as the reduction factors [16], the internal variables $D_k \in [0,1]$ being normalized scalars referred to as the damage variables for the matrix, D_m, and the two families of fibres, D_{f1} and D_{f2}, respectively [26].

Standard arguments, based on the Clausius–Duhem inequality $\mathscr{D}_{\text{int}} = -\dot{\Psi} + \frac{1}{2}\mathbf{S}:\dot{\mathbf{C}} \geqslant 0$, lead to the following representation

$$\mathbf{S} = 2\frac{\partial\Psi(\mathbf{C},\mathbf{M},\mathbf{N},D_k,\mathbf{Q}_{ik})}{\partial\mathbf{C}} = Jp\mathbf{C}^{-1} + J^{-2/3}\sum_{k=m,f_1,f_2}\text{DEV}\left[2(1-D_k)\frac{\partial\bar{\Psi}^0_k(\bar{\mathbf{C}},\mathbf{M},\mathbf{N})}{\partial\bar{\mathbf{C}}} - \sum_{i=1}^{N}\mathbf{Q}_{ik}\right]$$
$$= \mathbf{S}_{\text{vol}} + \sum_{k=m,f_1,f_2}\left\{\bar{\mathbf{S}}^0_k - J^{-2/3}\sum_{i=1}^{N}\text{DEV}\,\mathbf{Q}_{ik}\right\} \tag{11}$$

$$\mathscr{D}_{\text{int}} = \sum_{k=m,f_1,f_2}\left\{f_k\dot{D}_k + \sum_{i=1}^{N}\left[\frac{1}{2}\bar{\mathbf{C}} - \frac{\partial\Xi(\mathbf{Q}_{ik})}{\partial\mathbf{Q}_{ik}}\right]:\dot{\mathbf{Q}}_{ik}\right\} \geqslant 0 \tag{12}$$

with $\bar{\Psi}^0_k$ $(k=m, f_1, f_2)$ being the contributions of the matrix and the two families of fibres, respectively, and f_k conjugate state functions of the internal variables D_k defined as

$$f_m = \bar{\Psi}^0_m(\bar{\mathbf{C}}) \geqslant 0, \quad f_{f_1} = \bar{\Psi}^0_{f_1}(\bar{\mathbf{C}},\mathbf{M}) \geqslant 0, \quad f_{f_2} = \bar{\Psi}^0_{f_2}(\bar{\mathbf{C}},\mathbf{N}) \geqslant 0 \tag{13}$$

Copyright © 2007 John Wiley & Sons, Ltd.

DOI: 10.1002/nme

Since $\boldsymbol{\sigma}=(1/J)\mathbf{F}\mathbf{S}\mathbf{F}^{\mathrm{T}}$, the spatial description of expression (11) may be recast in the form

$$\boldsymbol{\sigma}=p\mathbf{1}+\frac{1}{J}\sum_{k=m,f_1,f_2}\operatorname{dev}\left[\bar{\mathbf{F}}\left\{2(1-D_k)\frac{\partial\bar{\Psi}_k^0(\bar{\mathbf{C}},\mathbf{M},\mathbf{N})}{\partial\bar{\mathbf{C}}}-\sum_{i=1}^{N}\mathbf{Q}_{ik}\right\}\bar{\mathbf{F}}^{\mathrm{T}}\right] \tag{14}$$

where p is the hydrostatic pressure $p=\mathrm{d}\Psi_{\mathrm{vol}}(J)/\mathrm{d}J$.

The non-equilibrium second Piola–Kirchhoff stresses in (11), $\mathbf{Q}_{ik}$, are assumed to be governed by a set of linear rate equations [25]:

$$\begin{aligned}&\dot{\mathbf{Q}}_{ik}+\frac{1}{\tau_{ik}}\mathbf{Q}_{ik}=\frac{\gamma_{ik}}{\tau_{ik}}(1-D_k)\operatorname{DEV}\left[2\frac{\partial\bar{\Psi}_k^0(\bar{\mathbf{C}},\mathbf{M},\mathbf{N})}{\partial\bar{\mathbf{C}}}\right]\\&\lim_{t\to-\infty}\mathbf{Q}_{ik}=\mathbf{0}\end{aligned} \tag{15}$$

where $\gamma_{ik}\in[0,1]$ are free energy factors associated with the relaxation times $\tau_{ik}>0$.

The evolution equations (15) are linear and, therefore, explicitly lead to the following convolution representation:

$$\mathbf{Q}_{ik}(t)=\frac{\gamma_{ik}}{\tau_{ik}}\int_{-\infty}^{t}\exp\left[\frac{-(t-s)}{\tau_{ik}}\right](1-D_k)\operatorname{DEV}\left[2\frac{\partial\bar{\Psi}_k^0}{\partial\bar{\mathbf{C}}}\right]\mathrm{d}s \tag{16}$$

3.2. Damage evolution

We assume that the damage mechanism is associated with the distortional energy and is independent of the hydrostatic pressure. Therefore, we define a damage criterion in the strain space by the condition that, at any time t of the loading process, the following expression is fulfilled [16]:

$$\phi_k(\mathbf{C}(t),\Xi_{k_t})=\sqrt{2\bar{\Psi}_k^0(\bar{\mathbf{C}}(t))}-\Xi_{k_t}=\Xi_k-\Xi_{k_t}\leqslant 0 \tag{17}$$

where $\bar{\mathbf{C}}(s)$ is the modified right Cauchy–Green tensor at time s and Ξ_{k_t} are defined as follows:

$$\Xi_{k_t}=\max_{s\in(-\infty,t)}\sqrt{2\bar{\Psi}_k^0(\bar{\mathbf{C}}(s))} \tag{18}$$

The equation $\phi_k(\mathbf{C}(t),\Xi_{k_t})=0$ defines a damage surface in the strain space [26]. Finally, the evolution of the damage parameters D_k is characterized by an irreversible equation of evolution

$$\frac{\mathrm{d}D_k}{\mathrm{d}t}=\begin{cases}\bar{h}_k(\Xi_k,D_k)\dot{\Xi}_k & \text{if } \phi=0 \text{ and } \mathbf{N}_k:\dot{\mathbf{C}}>0\\ 0 & \text{otherwise}\end{cases} \tag{19}$$

Here $\mathbf{N}_k:=\partial\phi_k/\partial\mathbf{C}$ is the normal to the damage surface in the strain space, Ξ_k are defined at the current time s, and $\bar{h}_k(\Xi_k,D_k)$ are given functions that characterize damage evolution in the material. In the case of $\bar{h}_k$ independent of D_k, the deviatoric part of the second Piola–Kirchhoff

Copyright © 2007 John Wiley & Sons, Ltd.

DOI: 10.1002/nme

stress tensor may be expressed in the following form:

$$\bar{\mathbf{S}}_k(t) = \bar{g}_k(\Xi_{k_t}) 2 \frac{\partial \bar{\Psi}_k^0(\bar{\mathbf{C}}(t))}{\partial \mathbf{C}} \tag{20}$$

with $\bar{h}_k(\Xi_k) = -\mathrm{d}\bar{g}_k(\Xi_k)/\mathrm{d}\Xi_k = -\bar{g}'_k$.

In all the examples presented next, the damage functions proposed correspond to the expressions

$$\bar{g}_k(\Xi_{k_t}) = \begin{cases} 1 & \text{if } \Xi_{k_t} < \Xi^0_{\min_k} \\ 1 - \xi^2[1 - \beta_k(\xi^2 - 1)] & \text{if } \Xi^0_{\min_k} \leqslant \Xi_{k_t} \leqslant \Xi^0_{\max_k} \\ 0 & \text{if } \Xi_{k_t} > \Xi^0_{\max_k} \end{cases} \tag{21}$$

where $\xi = (\Xi_{k_t} - \Xi^0_{\min_k})/(\Xi^0_{\max_k} - \Xi^0_{\min_k})$ a dimensionless variable and $\Xi^0_{\min_k}$ are the variables (18) associated with the strain energies at initial damage for matrix and fibres, respectively, $\Xi^0_{\max_k}$ the variables (18) associated with the strain energy at total damage for matrix and fibres and β_k model parameters, see [26].

4. ALGORITHMIC ASPECTS

4.1. Recursive update of the stress deviator at Gauss points

Algorithmically, the constitutive model is appealing since Equation (15) can be evaluated *via* a simple recursion relation that was originally developed for finite strains by Simo [16]. In particular, if the material state is known at a time t_n and the deformation is known at a time $t_{n+1} = t_n + \Delta t$ with $\Delta t > 0$, we may write

$$\mathbf{S}_{n+1} = J_{n+1} p_{n+1} \mathbf{C}^{-1}_{n+1} + J^{-2/3}_{n+1} \sum_{k=m,f} \left[\left(1 - \sum_{i=1}^{N} \gamma_{ik} \right) (1 - D_{(k)n+1}) \bar{\mathbf{S}}^0_{(k)n+1} \right]$$

$$+ J^{-2/3}_{n+1} \sum_{k=m,f} \sum_{i=1}^{N} [\gamma_{ik} \{ \mathrm{DEV}[\mathbf{H}^{(ik)}_{n+1}] \}] \tag{22}$$

where the subscripts n and $n+1$ denote quantities evaluated at times t_n and t_{n+1} [16, 25], and $\mathbf{H}^{(ik)}_{n+1}$ are internal algorithmic history variables defined as

$$\mathbf{H}^{(ik)}_{n+1} = \exp\left[\frac{-\Delta t}{\tau_{ik}} \right] \mathbf{H}^{(ik)}_n + \exp\left[\frac{-\Delta t}{2\tau_{ik}} \right] \{ (1 - D_{(k)n+1}) \bar{\mathbf{S}}^0_{(k)n+1} - (1 - D_{(k)n}) \bar{\mathbf{S}}^0_{(k)n} \} \tag{23}$$

Note that the time discretization scheme (22) used for the calculation of the current value of the stress $\mathbf{S}_{n+1}$ requires the storage of $(N+1)$k symmetric second-order tensors $\mathbf{H}^{(ik)}_n$ and $\bar{\mathbf{S}}^0_{(k)n}$ and 2k scalars $D_{(k)n}$ and Ξ_{k_t} at the previous time $t = t_n$ at each Gauss point of the finite element mesh.

4.2. Decoupled representation of the elasticity tensor

The iterative Newton procedure to solve a non-linear finite element problem requires the determination of the consistent tangent material operator. This can be derived analytically for the given

Copyright © 2007 John Wiley & Sons, Ltd.

DOI: 10.1002/nme

material equation (8). The symmetric algorithmic material tensor is expressed as [16]

$$\begin{aligned}\mathbb{C}_{n+1} = \mathbb{C}^0_{\mathrm{vol}\,n+1} + \sum_{k=m,f_1,f_2} \Bigg[& (1-D_{(k)n+1})(1-\gamma_k+\nu_k)\bar{\mathbb{C}}^0_{(k)n+1} \\ & -\frac{2}{3} J_{n+1}^{-4/3} \sum_{i=1}^{N} \gamma_{ik} \Bigg\{ \mathrm{DEV}[\tilde{\mathbf{H}}^{(ik)}_n] \otimes \bar{\mathbf{C}}^{-1}_{n+1} + \bar{\mathbf{C}}^{-1}_{n+1} \otimes \mathrm{DEV}[\tilde{\mathbf{H}}^{(ik)}_n] \\ & -(\tilde{\mathbf{H}}^{(ik)}_n : \bar{\mathbf{C}}) \left(\mathbb{I}^{-1}_{\mathbf{C}_{n+1}} - \frac{1}{3} \bar{\mathbf{C}}^{-1}_{n+1} \otimes \bar{\mathbf{C}}^{-1}_{n+1} \right) \Bigg\} - \bar{\mathbb{S}}_{(k)n+1} \Bigg]\end{aligned} \tag{24}$$

where $(\mathbb{I}^{-1}_{\mathbf{C}})_{ijkl} = -\frac{1}{2}(C^{-1}_{ik}C^{-1}_{jl} + C^{-1}_{il}C^{-1}_{jk})$ and

$$\bar{\mathbb{S}}_{(k)n+1} = \begin{cases} \bar{g}'_{(k)n+1} \bar{\mathbf{S}}^0_{(k)n+1} \otimes \bar{\mathbf{S}}^0_{(k)n+1} & \text{if } \phi = 0 \text{ and } \mathbf{N}_k : \dot{\mathbf{C}} > 0 \\ 0 & \text{otherwise} \end{cases} \tag{25}$$

and

$$\tilde{\mathbf{H}}^{(ik)}_n = \exp\left[\frac{-\Delta t}{\tau_{ik}}\right] \mathbf{H}^{(ik)}_n - \exp\left[\frac{-\Delta t}{2\tau_{ik}}\right] (1-D_{(k)n}) \bar{\mathbf{S}}^0_{(k)n} \tag{26}$$

where $\gamma_k = \sum_{i=1}^{N} \gamma_{ik}$, $\nu_k = \sum_{i=1}^{N} \gamma_{ik} \exp[-\Delta t/2\tau_{ik}]$.

For the reader's convenience, we have summarized the developed algorithm in Table I.

5. NUMERICAL EXAMPLES

The numerical algorithm presented in the previous sections has been implemented into the general-purpose finite element program ABAQUS [34] by means of a user subroutine UMAT. In order to illustrate the performance and the physical mechanisms involved in the constitutive model presented herein, we analysed three numerical examples. The aim of the first two is to show the basic behaviour of the anisotropic visco-hyperelastic-damage model in simple cases. The last example corresponds to an application in soft tissues. In all the examples we omit the dependency of the free energy function Ψ on I_5, I_7, I_8 and I_9 in order to reduce the number of material parameters and to work with physically motivated invariants.

The particular form of the deviatoric functions $\bar{\Psi}^m_0$ and $\bar{\Psi}^f_0$ is defined in (27) [35] and the volumetric part of the strain energy function is always stated as $\Psi_{\mathrm{vol}} = (1/D)\ln^2(J)$ [31]. The damage functions for the matrix and fibres were those established in (21):

$$\begin{aligned} \bar{\Psi}^0_m &= C_1(\bar{I}_1 - 3) \\ \bar{\Psi}^0_{f1} &= \frac{C_3}{C_4}(\exp^{C_4(\bar{I}_4-1)} - C_4(\bar{I}_4 - 1) - 1) \\ \bar{\Psi}^0_{f2} &= \frac{C_5}{C_6}(\exp^{C_6(\bar{I}_6-1)} - C_6(\bar{I}_6 - 1) - 1) \end{aligned} \tag{27}$$

Copyright © 2007 John Wiley & Sons, Ltd.

DOI: 10.1002/nme

Table I. Algorithmic procedure.

1. Database at each Gaussian point
   $\bar{\mathbf{S}}^0_{(k)n}$, $\mathbf{H}^{(ik)}_n$, $D_{(k)n}$, Ξ_{k_t} $i=1\ldots N$ internal viscoelastic variables and $k=m, f_1, f_2$
2. Compute the initial elastic stress tensors
   $$\mathrm{dev}[\boldsymbol{\sigma}^0_{(k)n+1}]=\frac{1}{J_{n+1}}\,\mathrm{dev}\left\{\bar{\mathbf{F}}_{n+1}\left[2\frac{\partial\bar{\Psi}^0_{(k)n+1}(\bar{\mathbf{C}}_{n+1},\mathbf{M},\mathbf{N})}{\partial\bar{\mathbf{C}}_{n+1}}\right]\bar{\mathbf{F}}^{\mathrm{T}}_{n+1}\right\}$$
   $$\bar{\mathbf{S}}^0_{(k)n+1}\bar{\mathbf{F}}_{n+1}(J_{n+1}\,\mathrm{dev}[\boldsymbol{\sigma}^0_{(k)n+1}])\bar{\mathbf{F}}^{\mathrm{T}}_{n+1}$$
3. Compute the current equivalent measure $\Xi_{k(n+1)}=\sqrt{2\bar{\Psi}^0_{k(n+1)}}$
4. Check the damage criterion
   $$\phi_{(k)n+1}(\mathbf{C}_{n+1},\Xi_{k_t})=\sqrt{2\bar{\Psi}^0_{(k)(n+1)}}-\Xi_{k_t}=\Xi_{(k)n+1}-\Xi_{k_t}>0$$
   YES: update damage internal variables
   $$1-D_{(k)n+1}=1-\xi^2[1-\beta_k(\xi^2-1)]\ \text{and}\ \bar{\mathbb{S}}_{(k)n+1}=\bar{g}'_{(k)n+1}\bar{\mathbf{S}}^0_{(k)n+1}\otimes\bar{\mathbf{S}}^0_{(k)n+1}$$
   NO: no additional damage
   $$D_{(k)n+1}=D_{(k)n}\ \text{and}\ \bar{\mathbb{S}}_{(k)n+1}=0$$
5. Update the viscoelastic internal variables
   $$\tilde{\mathbf{H}}^{(ik)}_n=\exp\left[\frac{-\Delta t}{\tau_{ik}}\right]\mathbf{H}^{(ik)}_n-\exp\left[\frac{-\Delta t}{2\tau_{ik}}\right](1-D_{(k)n})\bar{\mathbf{S}}^0_{(k)n}$$
   $$\mathbf{H}^{(ik)}_{n+1}=\tilde{\mathbf{H}}^{(ik)}_n+\exp\left[\frac{-\Delta t}{2\tau_{ik}}\right](1-D_{(k)n+1})\bar{\mathbf{S}}^0_{(k)n+1}$$
6. Compute the Cauchy stress tensor
   $$p_{n+1}=\left.\frac{\mathrm{d}\Psi_{\mathrm{vol}}(J_{n+1})}{\mathrm{d}J}\right|_{n+1}$$
   $$\tilde{\mathbf{h}}^{(k)}_n\sum_{i=1}^{N}\gamma_{ik}\,\mathrm{dev}[\bar{\mathbf{F}}_{n+1}\tilde{\mathbf{H}}^{(ik)}_n\bar{\mathbf{F}}^{\mathrm{T}}_{n+1}]$$
   $$\tilde{h}^{(k)}_n=\sum_{i=1}^{N}\gamma_{ik}\,\mathrm{tr}[\bar{\mathbf{F}}_{n+1}\tilde{\mathbf{H}}^{(ik)}_n\bar{\mathbf{F}}^{\mathrm{T}}_{n+1}]$$
   $$\boldsymbol{\sigma}_{n+1}=p_{n+1}\mathbf{1}+\sum_{k=m,f_1,f_2}\left[(1-\gamma_k+v_k)(1-D_{(k)n+1})\,\mathrm{dev}[\boldsymbol{\sigma}^0_{(k)n+1}]+\frac{1}{J_{n+1}}\tilde{\mathbf{h}}^{(k)}_n\right]$$
7. Compute the initial elastic modulus
   $\mathbb{C}^0_{\mathrm{vol}\,n+1}$ and $\bar{\mathbb{C}}^0_{(k)n+1}$
8. Introduce the viscoelastic effects
   $$\bar{\mathbb{C}}_{n+1}=\sum_{k=m,f_1,f_2}\Bigg[D_{(k)n+1}(1-\gamma_k+v_k)\bar{\mathbb{C}}^0_{(k)n+1}$$
   $$-\frac{2}{3J_{n+1}}[\tilde{\mathbf{h}}^{(j)}_n\otimes\mathbf{1}_{n+1}+\mathbf{1}\otimes\tilde{\mathbf{h}}^{(j)}_n-\tilde{h}^{(j)}_n(\mathbb{I}-\tfrac{1}{3}\mathbf{1}\otimes\mathbf{1})]-\bar{\mathbb{S}}_{(k)n+1}\Bigg]\quad\text{with}\ \bar{\mathbb{S}}=J^{-1}\boldsymbol{\chi}_*(\bar{\mathbb{S}})$$
9. Compute the elastic modulus
   $$\mathbb{C}_{n+1}=\mathbb{C}^0_{\mathrm{vol}\ n+1}+\bar{\mathbb{C}}_{n+1}$$

Copyright © 2007 John Wiley & Sons, Ltd.

DOI: 10.1002/nme

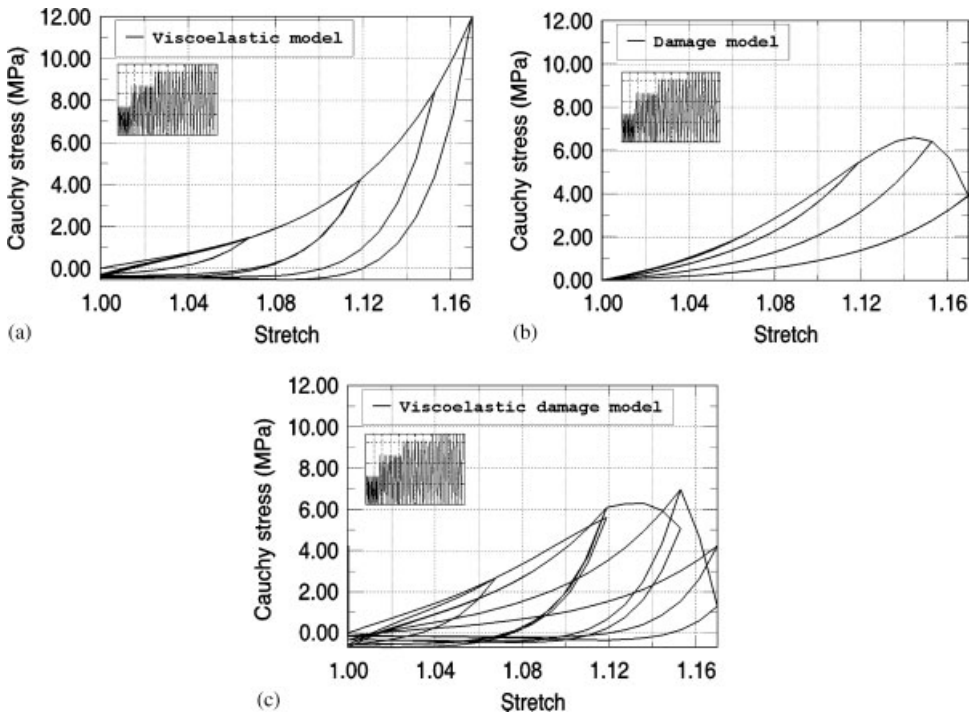

Figure 1. Stress response under cyclic simple tension: (a) viscoelastic material model; (b) elastic softening model; and (c) viscoelastic softening model.

5.1. Influence of damage on the stress–strain time-dependent response: uniaxial simple tension

In this example we show some differences between the presented viscoelastic model with and without damage [25]. For the purpose of comparison we consider a material with only one set of internal variables $N=1$. The stress response for a cyclic simple uniaxial tension test of a transversely isotropic material stretched along its longitudinal fibre axes is numerically simulated (see Figure 1). Four cyclic stretch histories with different mean stretches $\lambda_1=1.068$, $\lambda_2=1.119$, $\lambda_3=1.153$ and $\lambda_4=1.17$ are applied. In each phase, 10 cycles are carried out at a constant rate of $1.5\%\,\mathrm{s}^{-1}$. Afterwards, the strain is removed. The results of a purely viscoelastic behaviour [25], a purely damaged elastic case [26] and the coupled viscoelastic-damage model considered here were compared using the same material parameters shown in Table II under cyclic uniaxial tension.

In the purely viscoelastic case, it is easier to detect the damping behaviour and the associated hysteresis, but without stiffness reduction, Figure 1(a). In contrast, under purely elastic damage, softening effects can be observed, but other dissipative properties are neglected, Figure 1(b). In Figure 1(c) the characteristic Mullins's damage shows up very clearly. Under cyclic constant strain (i.e. with constant mean strain and strain amplitude), Mullins's damage increases only during the first cycles, i.e. after several cycles damage remains practically constant; hence, its value depends only on the maximal strain of the strain history. In addition, it can be observed that the stress response shows clearly a hysteretic effect within the deformation cycles and the stress does not recover its initial state.

Copyright © 2007 John Wiley & Sons, Ltd.

DOI: 10.1002/nme

Table II. Viscoelastic damage parameters for the uniaxial example.

C_1	C_2	C_3	C_4	C_5	C_6	D
1	0.0	0.4022	8.1390	0.0	0.0	0.000888
γ_m	τ_m	γ_{f1}	τ_{f1}	γ_{f2}	τ_{f2}	
0.307257	0.15	0.692743	5	—	—	
$\Xi^m_{\min}$	$\Xi^m_{\max}$	β^m	$\Xi^f_{\min}$	$\Xi^f_{\max}$	β^f	
0.0	0.439937	0.120	0.0	1.412501	0.1538	

Note: C_1, C_2, C_3, C_5 and Ξ^k are in MPa, D is in MPa^{-1}, τ_k in seconds and the rest of parameters are dimensionless.

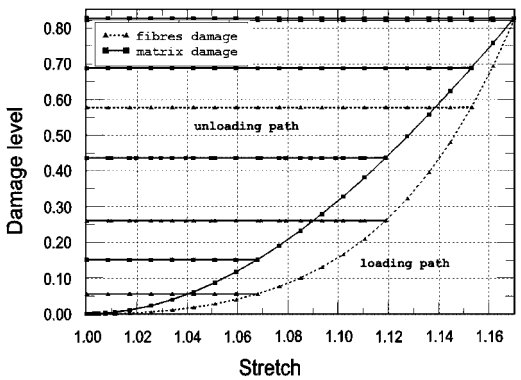

Figure 2. Damage evolution in matrix and fibres.

Figure 2 shows the damage evolutions for matrix and fibres. It can be seen that damage increases faster in the matrix than in the fibres due to the condition $\beta^m < \beta^f$. However, the corresponding damage peak values for the matrix and fibres resulted in 0.83 and 0.82, respectively.

5.2. Influence of the strain rate on the stress–strain response: biaxial tension

A biaxial test on a plane strain problem is presented in this example. Two cases are studied. In the first, only one family of fibres is defined along the X direction. In the second, two families of fibres are defined in the X and Y directions with different damage parameters. The specimen is subjected to cyclic stretching in the X and Y directions at three different strain rates ($0.05\%\,\text{s}^{-1}$, $5\%\,\text{s}^{-1}$ and $50\%\,\text{s}^{-1}$). The strain energy density function employed is the one in (27) with the material parameters included in Table III. These parameters were chosen in order to show the different viscoelastic behaviours of the matrix and the fibers.

Figure 3 shows the stress response obtained for case 1 at different strain rates. Since the fibres run along the X direction, the stress–strain response in this direction, $\sigma_x - \lambda_x$, mainly corresponds to the fibre behaviour while in the Y direction, $\sigma_y - \lambda_y$, the stress–strain response corresponds to the matrix (see Figures 3(a) and (b), respectively). The different elastic, viscoelastic and damage behaviours of the components are clearly appreciated, being the dissipative effects especially

Copyright © 2007 John Wiley & Sons, Ltd.

DOI: 10.1002/nme

Table III. Viscoelastic damage parameters for the biaxial example.

C_1	C_2	C_3	C_4	C_5	C_6	D		
1	0.0	0.4022	8.1390	0.4022	8.1390	0.000888		
γ_m	τ_m	γ_{f_1}	τ_{f_1}	γ_{f_2}	τ_{f_2}			
0.307257	3.25	0.692743	8.7	0.692743	8.7			
$\Xi^m_{\min}$	$\Xi^m_{\max}$	β^m	$\Xi^{f_1}_{\min}$	$\Xi^{f_1}_{\max}$	β^{f_1}	$\Xi^{f_2}_{\min}$	$\Xi^{f_2}_{\max}$	β^{f_2}
0.0	0.439937	0.120	0.0	1.412501	0.1538	0.523	1.1	0.1538

Note: C_1, C_2, C_3, C_5 and Ξ^k are in MPa, D is in MPa^{-1}, τ_k in seconds and the rest of parameters are dimensionless.

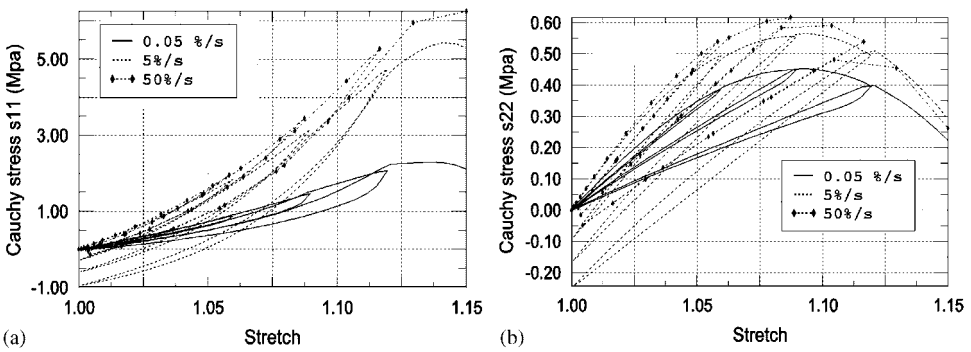

Figure 3. Biaxial stress response with one family of fibres: (a) σ_x and (b) σ_y.

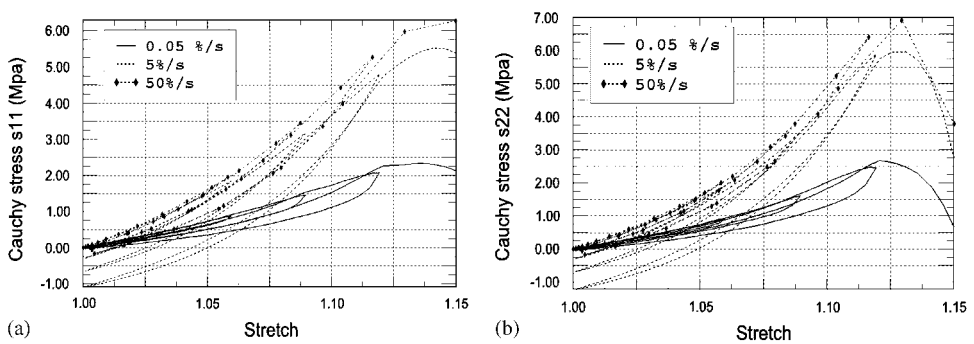

Figure 4. Biaxial stress response with two families of fibres: (a) σ_x and (b) σ_y.

remarkable. On the contrary, Figure 4 shows the stress response for the second case. The stress–strain path shows a similar pattern for both X and Y directions. However, the Mullin's effect on the global behaviour is clearly anisotropic due to $\psi^f_{\min}$ and $\psi^f_{\max}$ have different values for each direction.

Copyright © 2007 John Wiley & Sons, Ltd.

DOI: 10.1002/nme

The strain rate effect is clearly visible in the stress–strain curves in Figures 3 and 4. Tensile stresses depend upon the strain rate, being possible to recover pure elasticity for both very slow ($0.05\%\,s^{-1}$) and very fast ($50\%\,s^{-1}$) processes. However, at intermediate strain rates ($5\%\,s^{-1}$), the hysteresis loop is clearly visible. In addition, the influence of viscoelasticity on the rupture stress is also clear in all cases obtaining stiffer stress–strain curves and higher rupture stress at fast strain rates. This is especially relevant for the fibres for which the tensile strength at failure increases by 250% with an increase in the extension rate from 0.05 to $50\%\,s^{-1}$ (2.2–5.6 MPa). This effect has been reported in soft tissues with high collagen content such as ligaments and tendons [36].

5.3. Damage of human ligament under impact

Viscoelasticity of ligaments has been clearly demonstrated in creep and stress relaxation tests [23, 37–39]. There is, however, some variability in the findings of different studies performed to evaluate the change in ligament material properties with increasing loading rate. In those that analyse the effect of loading rates up to $400\%\,s^{-1}$, significant increases in stiffness [37, 40], load failure [36], and energy to failure [41] have been reported.

The purpose of this simulation is to demonstrate the effectiveness of the numerical algorithm and finite element implementation discussed in previous sections and the applicability of the model to simulate the structural behaviour of soft biological tissues. We reproduce in a human medial collateral ligament (MCL) the experiment developed by Woo *et al.* [42] in a rabbit MCL. The study was performed to determine the viscoelastic behaviour of ligaments at different loading rates, such as those associated with sports-related trauma.

The human model of the MCL was constructed to test quasi-static, physiological and impact conditions at displacement rates of 0.01; 1 and $113\,mm\,s^{-1}$ corresponding to strain rates of approximately 0.0025, 0.25 and $28\%\,s^{-1}$, respectively. The elastic, viscoelastic and damage parameters for the human MCL were fitted from published experimental data [22, 43] and are shown in Table IV. In order to adjust the experimental data, we firstly need to estimate the elastic parameters corresponding to quasi-static load in a uniaxial tension test. After that, $\Xi_{\min}$ and $\Xi_{\max}$ were assumed to correspond to the strain energy associated with the beginning and end of the damage process, respectively, in that quasi-static uniaxial test. We estimated β_m and β_f by fitting the damage evolution reported in [22]. Finally, the viscoelastic parameters were estimated by using the experimental data obtained for different strain rates also in uniaxial tension tests in [43]. The root mean square error obtained was 0.065 for a quasi-static uniaxial tension test with damages, 0.0822 and 0.237 for 50 and $1\%\,s^{-1}$ strain rates, respectively. Figure 5 shows the experimental results and the fitted curves.

Table IV. Viscoelastic damage parameters for the human MCL.

C_1	C_2	C_3	C_4	C_5	C_6	D
0.1539	0.0	0.1507	34.7929	0.0	0.0	3.986e−4
γ_m	τ_m	γ_{f1}	τ_{f1}	γ_{f2}	τ_{f2}	
0.4352	0.15	0.1500	2	—	—	
$\Xi^m_{\min}$	$\Xi^m_{\max}$	β^m	$\Xi^f_{\min}$	$\Xi^f_{\max}$	β^f	
0.0750	0.0932	0.120	0.3389	1.6652	0.1538	

Note: C_1, C_2, C_3, C_5 and Ξ^k are in MPa, D is in MPa^{-1}, τ_k in seconds and the rest of parameters are dimensionless.

Copyright © 2007 John Wiley & Sons, Ltd.

DOI: 10.1002/nme

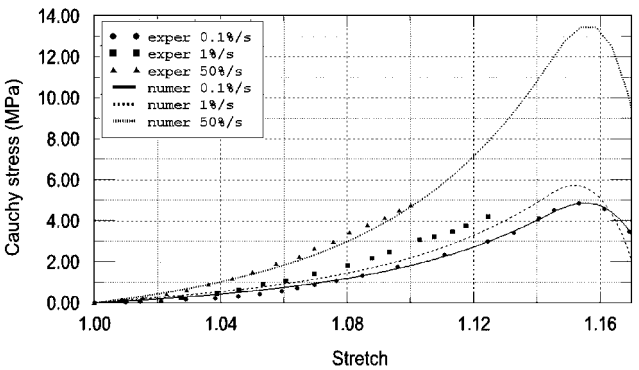

Figure 5. Stress–strain response of the human MCL at different displacement rates.

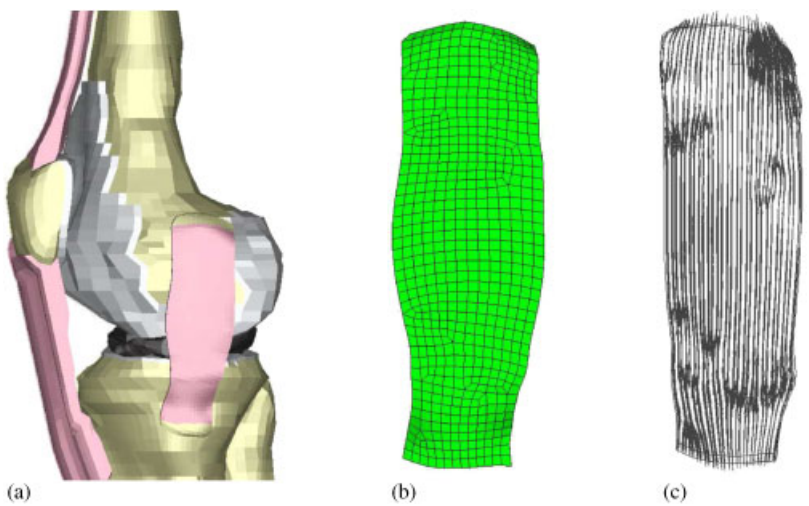

Figure 6. Finite element model of the human MCL: (a) model; (b) mesh; and (c) fiber distribution.

The surface geometries of the femur and tibia were reconstructed from a set of Computer Tomography scans, while for the MCL, magnetic resonance images (MRI) were used [6], see Figure 6. A total of 2448 nodes and 1510 eight-node brick elements were used to mesh the MCL. In all cases, we used trilinear hexahedral elements with a full geometrically non-linear formulation.

The load–elongation curves for the femur–MCL–tibia complex shown in Figure 7 were only slightly affected by the extension rate. In spite of the displacement rates in the impact testing ($113\,\mathrm{mm\,s^{-1}}$) being several orders of magnitude higher than the ones employed in the quasi-static test ($0.01\,\mathrm{mm\,s^{-1}}$), there were no large differences in the failure values. The loads to failure increased with increasing rates of extension, but the difference in the values obtained between the slowest and fastest rates was 23 N, which means an increment of only 16%. Similar results were obtained by Woo *et al.* [44] in a rabbit MCL. They tested it at the same displacement rates considered here. Despite the dramatic increase in displacement rate, they obtained an increase between the slowest and fastest rates in the load to failure of only 22%.

Copyright © 2007 John Wiley & Sons, Ltd.

DOI: 10.1002/nme

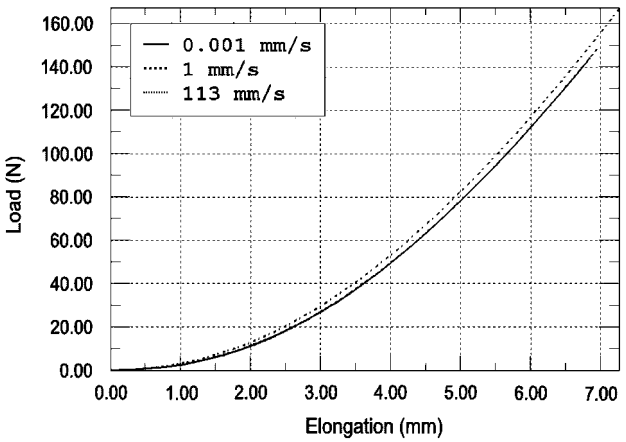

Figure 7. Load-displacement curves of the human MCL determined at different displacement rates.

Damage distributions in matrix and fibres at 0.01 and 113 mm s^{-1} of displacement rates are presented in Figure 8. In all cases, we considered failure of the MCL when damage reached a value of 0.6 for both matrix and fibres. We can observe the effect of the strain rate on the damage behaviour. At 113 mm s^{-1} of displacement rate, damage in matrix and fibres was much lower than that at 0.01 mm s^{-1}. This effect is especially evident in the fibres where damage decreased from 0.36 during the quasi-static test (0.01 mm s^{-1}) to 0.24 in the impact test (113 mm s^{-1}). The peak values appeared in the ligament substance (contact region between ligament and tibial plate), as also has been reported in previous experimental studies [44, 45]. Damage during distraction usually appears in that region.

6. CONCLUSIONS

This paper presents a coupled visco-hyperelastic-damage model to analyse the strain-softening time-dependent behaviour of fibrous soft tissues and in particular of ligaments. The research question addressed in the paper is to assess whether, in the framework of the class of phenomenological models, a time-dependent constitutive damage model with viscoelastic properties different for matrix and reinforcing fibres can predict different experimental evidences in these types of materials [43]. On the numerical side, a general procedure for the simulation of finite-strain problems involving dissipative fibred materials has been described in detail. Emphasis has been placed on the numerical treatment of the proposed formulation in the context of the finite element method and particular attention has been paid to the derivation of the corresponding tangent tensor, essential for the solution of the implicit finite element equations. We have presented an implicit second-order accurate integration algorithm that trivially satisfies objectivity requirements under superposed rigid-body motions.

By means of several examples, the good performance and the physical mechanisms inherent to the constitutive model presented herein have been shown. A set of finite element simulations of the stress responses of simple tests of biological tissues have been carried out under cyclic loading conditions. These examples show that the proposed material law is able to characterize the

Copyright © 2007 John Wiley & Sons, Ltd.

DOI: 10.1002/nme

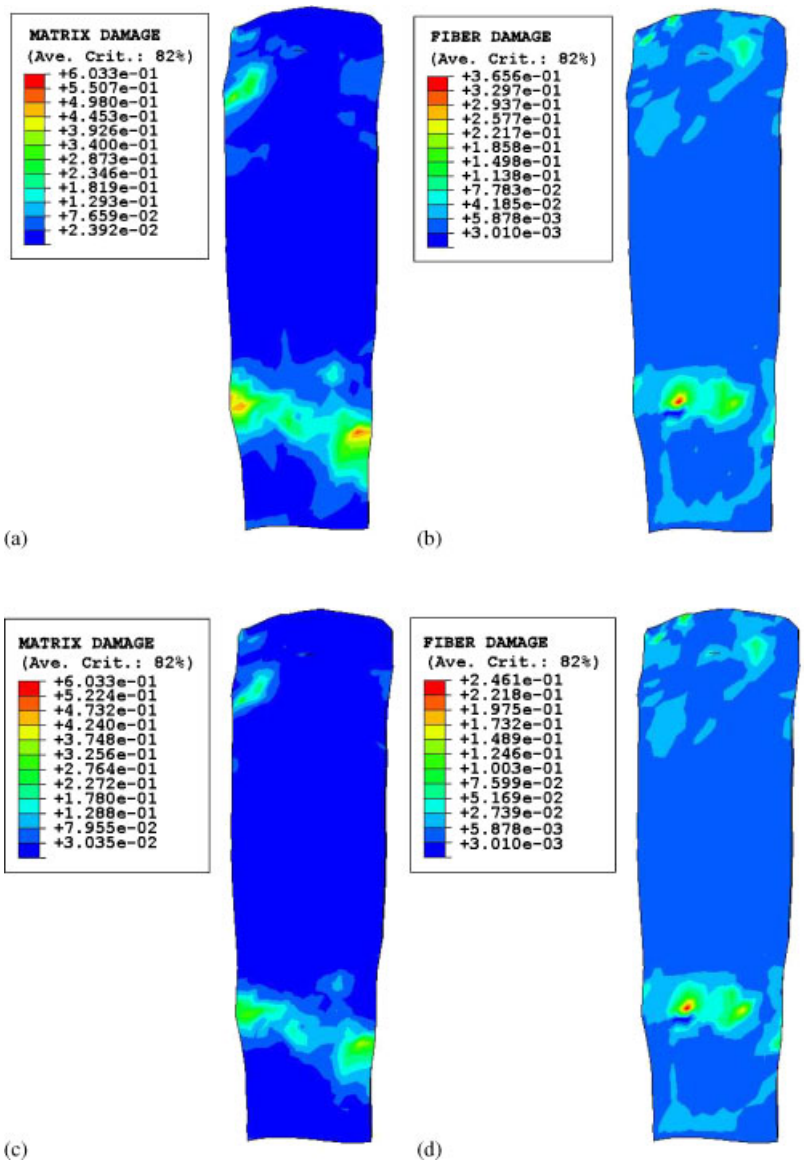

Figure 8. Damage in a human MCL under different displacement rates: (a) matrix damage at $0.01\,\mathrm{mm\,s^{-1}}$; (b) fibre damage at $0.01\,\mathrm{mm\,s^{-1}}$; (c) matrix damage at $113\,\mathrm{mm\,s^{-1}}$; and (d) fibre damage at $113\,\mathrm{mm\,s^{-1}}$.

constitutive responses of soft biological tissues effectively. The example corresponding to a uniaxial tension test (Figure 1(a)) shows that the visco-hyperelastic-damage model is appropriate to model the characteristics of strain-rate softening of biological tissues [22, 43, 46, 47]. The biaxial example shows the model ability to capture the different viscoelastic and damage behaviour for matrix and

Copyright © 2007 John Wiley & Sons, Ltd.

DOI: 10.1002/nme

fibres. The strain-rate effect is visible in the stress–strain curves presented in Figures 3 and 4. This is clear from the stiffer stress–strain curves and the higher rupture stress detected for fast strain rates. This has been reported in soft tissues with high collagen content as ligaments and tendons [36]. We also analysed the three-dimensional behaviour of the MCL under non-physiological distraction, reproducing in the human MCL the experiment developed by Woo *et al.* [44] in a rabbit MCL. Good qualitative agreement was been found between the numerical and experimental results for the MCL, indicating that the constitutive viscoelastic-damage model can capture the typical stress–strain behaviour observed in fibrous soft tissues. Note that the obtained results are qualitative. Ideally the material parameters and geometry of the MCL should be obtained from one subject. However, the experimental results used to fit the material parameters correspond to human experiments from published data [22, 43] and the solid models of femur and tibia are the same that the authors used in a previous work [6]. Hence, this example does not exactly correspond to a validation problem although it gives sufficient indications about the accuracy and possibilities of the model [3].

To our knowledge although there are some other linear [9, 10, 25, 48, 49] or non-linear [50, 51] viscoelastic models for soft biological tissues, none of them includes the softening behaviour of these materials. On the other hand, there are some other works that include damage of soft tissues [26, 27, 46]. Only Arnoux *et al.* [22] presented a viscoelastic-damage model for ligaments, although they did consider ligaments as isotropic with an isotropic evolution of the viscoelastic and damage variables.

The present study has however some important limitations. The most remarkable is the need of a suitable experimental plan to obtain the many parameters involved. Another limitation is that the evolution equations of the viscoelastic internal variables ($\mathbf{Q}_{ik}$) are linear (15). It is known that the viscoelastic behaviour of soft biological tissues and in particular of ligaments and tendons is non-linear [38, 43, 52]. Finally, we cannot simulate visible injuries that imply tearing of the tissue with the damage model presented herein that follows a continuum approach. In the near future, we plan to complete this phenomenological model with the following subjects. First, we will formulate the evolution equations for the viscoelastic variables in a non-linear form to take into account the non-linear viscoelastic behaviour of soft biological tissues. In addition, we need to compare model performance with experimental results in order to obtain a quantitative validation. In spite of all these limitations, a good qualitative agreement was found between numerical and some experimental results in the literature, indicating that the constitutive viscoelastic-damage model can capture the typical stress–strain behaviour observed in fibrous soft tissue. Some possible applications may be mentioned such as sports (skiing, basketball, soccer) and traffic accidents that are the most important causes of ligament injury. In fact, the strain rate during injury is very important regarding the magnitude of the lesion [53]. Vascular surgery simulations (balloon angioplasty, arterial clamping or stenting), corneal laser interventions or plastic surgery are other interesting applications to be considered in the near future.

APPENDIX A: DERIVATION OF THE EXPRESSION FOR THE STRESS AND ELASTICITY TENSORS

In this appendix, we derive the expression for the stress in the recursive algorithm presented in Section 4. Substitution of (15) into (11) and integrating by parts yields the following equivalent

Copyright © 2007 John Wiley & Sons, Ltd.

DOI: 10.1002/nme

expression:

$$\mathbf{S} = Jp\mathbf{C}^{-1} + J^{-2/3} \sum_{k=m,f_1,f_2} \left[\left(1 - \sum_{i=1}^{N} \gamma_{ik} \right) \mathrm{DEV} \left\{ 2(1-D_k) \frac{\partial \bar{\Psi}_k^0(\bar{\mathbf{C}}, \mathbf{M}, \mathbf{N})}{\partial \bar{\mathbf{C}}} \right\} \right]$$
$$+ \sum_{k=m,f_1,f_2} \sum_{i=1}^{N} \left[J^{-2/3} \gamma_{ik} \int_{-\infty}^{t} \exp\left[\frac{-(t-s)}{\tau_{ik}} \right] \frac{\mathrm{d}}{\mathrm{d}s} \left\{ \mathrm{DEV} \left[2(1-D_k) \frac{\partial \bar{\Psi}_k^0(\bar{\mathbf{C}}, \mathbf{M}, \mathbf{N})}{\partial \bar{\mathbf{C}}} \right] \right\} \mathrm{d}s \right] \tag{A1}$$

The convolution representation (A1) in terms of the Cauchy stress tensor takes the form

$$\boldsymbol{\sigma} = p\mathbf{1} + \frac{1}{J} \left[\sum_{k=m,f_1,f_2} \left[\left(1 - \sum_{i=1}^{N} \gamma_{ik} \right) \mathrm{dev} \left\{ \bar{\mathbf{F}} \left[2(1-D_k) \frac{\partial \bar{\Psi}_k^0(\bar{\mathbf{C}}, \mathbf{M}, \mathbf{N})}{\partial \bar{\mathbf{C}}} \right] \bar{\mathbf{F}}^{\mathrm{T}} \right\} \right] \right.$$
$$\left. + \sum_{i=1}^{N} \sum_{k=m,f_1,f_2} \left[\gamma_{ik} \int_{-\infty}^{t} \exp\left[\frac{-(t-s)}{\tau_{ik}} \right] \frac{\mathrm{d}}{\mathrm{d}s} \left\{ \mathrm{dev} \left\{ \bar{\mathbf{F}} \left[2(1-D_k) \frac{\partial \bar{\Psi}_k^0(\bar{\mathbf{C}}, \mathbf{M}, \mathbf{N})}{\partial \bar{\mathbf{C}}} \right] \bar{\mathbf{F}}^{\mathrm{T}} \right\} \right\} \right] \mathrm{d}s \right] \tag{A2}$$

For the purpose of numerical integration, we need to transform the convolution representation (A1) into a two-step recursive formula involving internal variables stored at the quadrature points of a finite element mesh [33]. We introduce the following internal algorithmic history variables:

$$\mathbf{H}^{(ik)} = \int_{-\infty}^{t} \exp\left[\frac{-(t-s)}{\tau_{ik}} \right] \frac{\mathrm{d}}{\mathrm{d}s} \left\{ \mathrm{DEV} \left[2(1-D_k) \frac{\partial \bar{\Psi}_k^0(\bar{\mathbf{C}}, \mathbf{M}, \mathbf{N})}{\partial \bar{\mathbf{C}}} \right] \right\} \mathrm{d}s \tag{A3}$$

From an algorithmic standpoint, the problem is defined in the usual strain-driven format and we assume that at certain times t_n and t_{n+1} all relevant kinematic quantities are known and consider $\Delta t_n = t_{n+1} - t_n$ as the associated time increment. Without loss of generality, we take $t_0 = -\infty$. Using the semi-group property of the exponential function, the property of additivity of the integral over the interval of integration and the midpoint rule to approximate the integral over $[t_n, t_{n+1}]$ we can arrive at the update formula (23) and the algorithmic approximation for the second Piola–Kirchhoff stress (22).

Also, we can calculate the Cauchy stress tensor as

$$\boldsymbol{\sigma}_{n+1} = p_{n+1}\mathbf{1} + \frac{1}{J_{n+1}} \sum_{k=m,f_1,f_2} \left[\left(1 - \sum_{i=1}^{N} \gamma_{ik} \right) \mathrm{dev} \left\{ \bar{\mathbf{F}}_{n+1} \left[2(1-D_{k(n+1)}) \frac{\partial \bar{\Psi}_k^0(\bar{\mathbf{C}}, \mathbf{M}, \mathbf{N})}{\partial \bar{\mathbf{C}}} \right] \bar{\mathbf{F}}_{n+1}^{\mathrm{T}} \right\} \right]$$
$$+ \frac{1}{J_{n+1}} \sum_{k=m,f_1,f_2} \sum_{i=1}^{N} [\gamma_{ik} \{ \mathrm{dev}[\bar{\mathbf{F}}_{n+1} [\mathbf{H}_{n+1}^{(ik)}] \bar{\mathbf{F}}_{n+1}^{\mathrm{T}}] \}] \tag{A4}$$

Copyright © 2007 John Wiley & Sons, Ltd.

DOI: 10.1002/nme

In order to obtain the elasticity tensor (24), we rewrite the update formula (23) as [33]

$$\tilde{\mathbf{H}}_n^{(ik)} = \exp\left[\frac{-\Delta t}{\tau_{ik}}\right]\mathbf{H}_n^{(ik)} - \exp\left[\frac{-\Delta t}{2\tau_{ik}}\right](1-D_{k(n)})\bar{\mathbf{S}}^0_{(k)n} \tag{A5}$$

$$\mathbf{H}_{n+1}^{(ik)} = \tilde{\mathbf{H}}_n^{(ik)} + \exp\left[\frac{-\Delta t}{2\tau_{ik}}\right](1-D_{k(n+1)})\bar{\mathbf{S}}^0_{(k)n+1} \tag{A6}$$

With this notation

$$\mathbf{S}_{n+1} = J_{n+1}p_{n+1}\mathbf{C}_{n+1}^{-1} + J_{n+1}^{-2/3}\sum_{k=m,f_1,f_2}\left[(1-\gamma_k+v_k)(1-D_{k(n+1)})\bar{\mathbf{S}}^0_{(k)n+1} + \sum_{i=1}^{n}\gamma_{ik}\{\mathrm{DEV}[\tilde{\mathbf{H}}_n^{(ik)}]\}\right] \tag{A7}$$

$$\boldsymbol{\sigma}_{n+1} = p_{n+1}\mathbf{1} + \sum_{k=m,f_1,f_2}\left[(1-\gamma_k+v_k)(1-D_{k(n+1)})\,\mathrm{dev}[\boldsymbol{\sigma}^0_{(k)n+1}] + \frac{1}{J_{n+1}}\sum_{i=1}^{n}\gamma_{ik}\{\mathrm{dev}[\tilde{\mathbf{h}}_n^{(ik)}]\}\right] \tag{A8}$$

The associated decoupled elasticity tensor (24) can be derived analytically for the given material equation (8) using the second Piola–Kirchhoff stress tensor (A7).

REFERENCES

1. Peña E, Martinez MA, Calvo B, Doblaré M. On the numerical treatment of initial strains in soft biological tissues. *International Journal for Numerical Methods in Engineering* 2006; **68**:836–860.
2. Holzapfel GA, Gasser TC. A viscoelastic model for fiber-reinforced composites at finite strains: continuum basis, computational aspects and applications. *Computer Methods in Applied Mechanics and Engineering* 2001; **190**:4379–4403.
3. Peña E, Pérez del Palomar A, Calvo B, Martínez MA, Doblaré M. Computational modelling of diarthrodial joints. Physiological, pathological and pos-surgery simulations. *Archives of Computational Methods in Engineering* 2007; **14**(1):1–54.
4. Spencer AJM. Theory of invariants. *Continuum Physics*. Academic Press: New York, 1954; 239–253.
5. Weiss JA, Maker BN, Govindjee S. Finite element implementation of incompressible, transversely isotropic hyperelasticity. *Computer Methods in Applied Mechanics and Engineering* 1996; **135**:107–128.
6. Peña E, Calvo B, Martinez MA, Doblaré M. A three-dimensional finite element analysis of the combined behaviour of ligaments and menisci in the healthy human knee joint. *Journal of Biomechanics* 2006; **39**(9):1686–1701.
7. Holzapfel GA, Gasser TC, Ogden RW. A new constitutive framework for arterial wall mechanics and a comparative study of material models. *Journal of Elasticity* 2000; **61**:1–48.
8. Alastrue V, Calvo B, Peña E, Doblare M. Biomechanical modelling of refractive corneal surgery. *Journal of Biomechanical Engineering* (ASME) 2006; **128**:150–160.
9. Puso MA, Weiss JA. Finite element implementation of anisotropic quasilinear viscoelasticity. *Journal of Biomechanical Engineering* (ASME) 1998; **120**:162–170.
10. Johnson GA, Livesay GA, Woo SLY, Rajagopal KIR. A single integral finite strain viscoelastic model of ligaments and tendons. *Journal of Biomechanical Engineering* (ASME) 1996; **118**:221–226.
11. Humphrey JD. Mechanics of the arterial wall: review and directions. *Critical Reviews in Biomedical Engineering* 1995; **23**:1–162.
12. Pinsky PM, Datye V. A microstructurally-based finite element model of the incised human cornea. *Journal of Biomechanics* 1991; **10**:907–922.

Copyright © 2007 John Wiley & Sons, Ltd.

DOI: 10.1002/nme

13. Hayes WC, Mockros LF. Viscoelastic constitutive relations for human articular cartilage. *Journal of Applied Physiology* 1971; **18**:562–568.
14. Mak A. The apparent viscoelastic behaviour of articular cartilage. The contributions from the intrinsic matrix viscoelastocity and intersticial fluid flows. *Journal of Biomechanical Engineering* (ASME) 1986; **108**:123–130.
15. Provenzano PP, Heisey D, Hayashi K, Lakes R, Vanderby R. Subfailure damage in ligament: a structural and cellular evaluation. *Journal of Applied Physiology* 2002; **92**:362–371.
16. Simo JC. On a fully three-dimensional finite-strain viscoelastic damage model: Formulation and computational aspects. *Computer Methods in Applied Mechanics and Engineering* 1987; **60**:153–173.
17. Govindjee S, Simo JC. Mullins' effect and the strain amplitude dependence of the storage modulus. *International Journal of Solids and Structures* 1992; **29**:1737–1751.
18. Kaliske M, Rothert H. Viscoelastic and elastoplastic damage formulations. *Constitutive Models for Rubber*. Balkema: Rotterdam, 1999; 159–167.
19. Kaliske M, Nasdala L, Rothert H. On damage modelling for elastic and viscoelastic materials at large strain. *Computers and Structures* 2001; **79**:2133–2141.
20. Canga ME, Becker EB, Özüpek S. Constitutive modeling of viscoelastic materials with damage—computational aspects. *Computer Methods in Applied Mechanics and Engineering* 2001; **190**:2207–2226.
21. Lin RC, Schomburg U. A finite-viscoelastic–elastoplastic material law with damage: theoretical and numerical aspects. *Computer Methods in Applied Mechanics and Engineering* 2003; **192**:1591–1627.
22. Arnoux PJ, Chabrand P, Jean M, Bonnoit J. A visco-hyperelastic with damage for the knee ligaments under dynamic constraints. *Computer Methods in Biomechanics and Biomedical Engineering* 2002; **5**:167–174.
23. Weiss JA, Gardiner JC, Bonifasi-Lista C. Ligament material behaviour is nonlinear, viscoelastic and rate-independent under shear loading. *Journal of Biomechanics* 2002; **35**:943–950.
24. Limbert G, Middleton J. A transversely isotropic viscohyperelastic material. Application to the modeling of biological soft connective tissues. *International Journal of Solids and Structures* 2004; **41**:4237–4260.
25. Peña E, Calvo B, Martínez MA, Doblaré M. An anisotropic visco-hyperelastic model for ligaments at finite strains: formulation and computational aspects. *International Journal of Solids and Structures* 2007; **44**:760–778.
26. Calvo B, Peña E, Martínez MA, Doblaré M. An uncoupled directional damage model for fibered biological soft tissues. Formulation and computational aspects. *International Journal for Numerical Methods in Engineering* 2007; **69**:2036–2057.
27. Rodríguez JF, Cacho F, Bea JA, Doblaré M. A stochastic-structurally based three dimensional finite-strain damage model for fibrous soft tissue. *Journal of the Mechanics and Physics of Solids* 2006; **54**:564–886.
28. Flory PJ. Thermodynamic relations for high elastic materials. *Transaction of the Faraday Society* 1961; **57**: 829–838.
29. Simo JC, Taylor RL. Quasi-incompressible finite elasticity in principal stretches. Continuum basis and numerical algorithms. *Computer Methods in Applied Mechanics and Engineering* 1991; **85**:273–310.
30. Simo JC, Taylor RL. Consistent tangent operators for rate-independent elastoplasticity. *Computer Methods in Applied Mechanics and Engineering* 1985; **48**:101–118.
31. Holzapfel GA. *Nonlinear Solid Mechanics*. Wiley: New York, 2000.
32. Marsden JE, Hughes TJR. *Mathematical Foundations of Elasticity*. Dover: New York, 1994.
33. Simo JC, Hughes TJR. *Computational Inelasticity*. Springer: New York, 1998.
34. Hibbit, Karlsson and Sorensen, Inc. *Abaqus User's Guide*, *v. 6.5*. HKS inc. Pawtucket, RI, U.S.A., 2006.
35. Natali AN, Pavan PG, Carniel EL, Luisiano ME, Taglialavoro G. Anisotropic elasto-damage constitutive model for the biomechanical analysis of tendons. *Medical Engineering and Physics* 2005; **27**:209–214.
36. Yamamoto K, Hirokawa S, Kawada T. Strain distribution in the ligamnet using photoelasticity. A direct application to the human ACL. *Medical Engineering and Physics* 1998; **20**:161–168.
37. Pioletti DP, Rakotomanana LR, Benvenuti J-F, Leyvraz P-F. Viscoelastic constitutive law in large deformations: application to human knee ligaments and tendons. *Journal of Biomechanics* 1998; **31**:753–757.
38. Provenzano PP, Lakes RS, Corr DT, Vanderby R. Application of nonlinear viscoelastic models to describe ligament behaviour. *Biomechanics and Modeling in Mechanobiology* 2002; **1**:45–47.
39. Puxkandl R, Zizak I, Paris O, Tesch W, Bernstorff S, Purslow P, Fratzl1 P. Viscoelastic properties of collagen: synchrotron radiation investigations and structural model. *Philosophical Transactions of the Royal Society of London Series B* 2002; **357**:191–197.
40. Danto MI, Woo SLY. The mechanical properties of skeletally mature rabbit anterior cruciate ligament and patellar tendon over range of strain rates. *Journal of Orthopaedic Research* 1993; **11**:58–67.
41. Noyes FR, DeLucas JL, Torvik PJ. Biomechanics of anterior cruciate ligament failure: an analysis of strain-rate sensitivity and mechanisms of failure in primates. *Journal of Bone Joint Surgery* 1974; **56**(A):236–253.

Copyright © 2007 John Wiley & Sons, Ltd.

DOI: 10.1002/nme

42. Woo SL-Y, Dedski RE, Zeminski J, Abramowitch SD, Chan SS, Fenwick JA. Injury and repair of ligaments and tendons. *Annual Review of Biomedical Engineering* 2000; **2**:83–118.
43. Bonifasi-Lista C, Lake SP, Small MS, Weiss JA. Viscoelastic properties of the human medial collateral ligament under longitudinal, transverse and shear loading. *Journal of Orthopaedic Research* 2005; **23**:67–76.
44. Woo SL-Y, Peterson RH, Ohland KJ, Sites TJ, Danto MI. The effects of strain rate on the properties of the medial collateral ligament in skeletally immature and mature rabbits: a biomechanical and histological study. *Journal of Orthopaedic Research* 1990; **8**:712–721.
45. Crisco JJ, Moore DC, McGovern RD. Strain-rate sensitivity of the rabbit MCL diminishes at traumatic loading rates. *Journal of Biomechanics* 2002; **35**:1379–1385.
46. Natali AN, Pavan PG, Carniel EL, Dorow C. A transversely isotropic elasto-damage constitutive model for the periodontal ligament. *Computer Methods in Biomechanics and Biomedical Engineering* 2003; **6**:329–336.
47. Yamamoto N, Hayashi K. Mechanical properties of rabbit patellar tendon at high strain rate. *Biomedical Materials and Engineering* 1998; **8**:83–90.
48. Holzapfel GA, Gasser TC, Stadler M. A structural model for the viscoelastic behaviour of arterial walls: continuum formulation and finite element analysis. *European Journal of Mechanics–A/Solids* 2002; **21**:441–463.
49. Jamison CE, Marangoni RD, Glaser AA. Viscoelastic properties of soft tissue by discrete model characterization. *Journal of Biomechanics* 1968; **1**:33–46.
50. Pioletti DP, Rakotomanana L, Leyvraz PF, Benvenuti JF. Finite element model of the anterior cruciate ligament. *Computer Methods in Biomechanics and Biomedical Engineering* 1997.
51. Vena P, Gastaldi D, Contro R. A constituent-based model for the nonlinear viscoelastic behaviour of ligaments. *Journal of Biomechanical Engineering* (ASME) 2006; **128**:449–457.
52. Hingorani RV, Provenzano PP, Lakes RS, Escarcega A, Vanderby Jr R. Nonlinear viscoelasticity in rabbit medial collateral ligament. *Annals of Biomedical Engineering* 2004; **32**:306–312.
53. Fu FH, Harner C, Vince KG. *Knee Surgery*. Williams and Wilkins: Baltimore, 1994.

Copyright © 2007 John Wiley & Sons, Ltd.

DOI: 10.1002/nme